American Mineralogist, Volume 72, pages 580–593, 1987

Characterization of synthetic pargasitic amphiboles ($NaCa_2Mg_4M^{3+}Si_6Al_2O_{22}(OH,F)_2$; M^{3+} = Al, Cr, Ga, Sc, In) by infrared spectroscopy, Rietveld structure refinement, and ^{27}Al, ^{29}Si, and ^{19}F MAS NMR spectroscopy

MATI RAUDSEPP, ALLAN C. TURNOCK, FRANK C. HAWTHORNE
Department of Geological Sciences, University of Manitoba, Winnipeg, Manitoba R3T 2N2, Canada
BARBARA L. SHERRIFF*
Department of Geological Sciences, Brock University, St. Catharines, Ontario L2S 3A1, Canada
J. STEPHEN HARTMAN
Department of Chemistry, Brock University, St. Catharines, Ontario L2S 3A1, Canada

ABSTRACT

Natural and synthetic amphiboles can display long-range and short-range order-disorder that must be characterized for proper interpretation of synthesis experiments. In this study, octahedral M^{3+} (Al, Cr, Ga, Sc, In) analogues of pargasite and fluor-pargasite were synthesized and characterized by optical and scanning-electron microscopy; X-ray diffraction; infrared spectroscopy; ^{27}Al, ^{29}Si, and ^{19}F magic-angle spinning (MAS) nuclear magnetic resonance (NMR) spectroscopy; and Rietveld structure analysis. Although "end-member" pargasite was synthesized readily, yields were never quite 100%; cell dimensions were consistent with previous studies. Substitution of Cr, Ga, Sc, and In for octahedral Al reduced yields to less than 90%. Variation in cell volume with the cube of the average octahedral cation radius for this isostructural series was not linear, indicating incomplete substitution of these cations for Al. For the pargasites, the infrared spectra showed that the octahedrally coordinated trivalent cations were significantly disordered over the M(1,2,3) sites of the octahedral strip. In the fluor-pargasites, the trivalent cations tended to be more strongly ordered at M(2). The ^{29}Si MAS NMR spectrum of scandium-fluor-pargasite was incompatible with complete ordering of tetrahedral Al at the T(1) site.

INTRODUCTION

One of the goals of experimental mineralogy is to grow minerals with specific compositions and structures under controlled conditions. By characterizing the products, mineral compositions and structures may be related quantitatively to growth conditions such as temperature and pressure. These data are vital to understanding the properties and phase relations of analogous natural minerals as a function of their environment.

Natural and synthetic amphiboles can display long-range and short-range order-disorder that must be characterized for proper interpretation of the results of synthesis experiments. Of specific importance here is cation order-disorder and chain-width order-disorder. This paper reports on the synthesis and characterization of octahedral M^{3+} analogues of pargasite and fluor-pargasite, part of a systematic study to critically assess the results of amphibole synthesis and to more adequately characterize the products (Raudsepp, 1984; Raudsepp et al., 1982; Raudsepp et al., 1984; Hawthorne et al., 1984). Our study was restricted to Fe-free, monoclinic amphiboles with the $C2/m$ structure because previous studies (e.g., Veblen, 1981; Maresch and Czank, 1983) show that Fe-Mg-Mn amphiboles are not only difficult to synthesize, but also are subject to short-range chain-width disorder, high densities of stacking faults, and other local structural disorder. There is at present no indication that such local structural disorder occurs in synthetic calcic and sodic amphiboles, but little work has been done on this problem.

Pargasites are monoclinic calcic amphiboles with the $C2/m$ structure (Hawthorne, 1983b). The ideal end-member formula of pargasite is $NaCa_2Mg_4AlSi_6Al_2O_{22}(OH)_2$. In this study, synthetic analogues with octahedral Al replaced by Ga, Cr, Sc, and In were grown for both the hydroxy- and fluor- end members. Run products were characterized by optical and scanning-electron microscopy (morphology; detection of foreign phases); X-ray diffraction (cell dimensions; detection of foreign phases); infrared spectroscopy (ordering); ^{27}Al, ^{29}Si, and ^{19}F MAS NMR spectroscopy (ordering and site occupancies); and Rietveld structure analysis (ordering and site occupancies).

* Present address: Department of Geology, McMaster University, Hamilton, Ontario L8S 4M1, Canada.

0003–004X/87/0506–0580$02.00

Previous studies

Many workers have synthesized (nominal) pargasite (Boyd, 1959; Gilbert, 1969; Holloway, 1973; Semet, 1973; Hinrichsen and Schürmann, 1977; Braue and Seck, 1977; Oba, 1980; Westrich and Holloway, 1981). Additional phases were often reported as present in minor amounts, but the cell dimensions reported generally agree fairly closely with each other. Boyd (1954) and Westrich and Navrotsky (1981) synthesized fluor-pargasite, again with minor amounts of additional phases present in the run products.

Experimental methods

Synthesis

Dry mixtures of the anhydrous amphibole stoichiometry were prepared from commercial reagents. SiO_2 was added as Corning Fused Silica Code 7940. The glass was crushed in a steel mortar, cleaned in aqua regia, washed in distilled water and dried at 1000°C. SiO_2 was added to certain fluor-pargasite mixes as dehydrated $H_2SiO_3 \cdot nH_2O$. $Al(OH)_3$ was heated at 900°C for 48 h to yield γ-Al_2O_3. MgO was dried at 1000°C to constant weight. For hydroxy-pargasites, either Ca was added as $CaCO_3$ that had been decarbonated to constant weight before weighing, or Ca was added to the mix as $CaCO_3$ and the whole mix was decarbonated at 1000°C. In fluor-pargasites, Ca was added as CaF_2. For hydroxy-pargasites, Na was added as $Na_2Si_2O_5$ prepared after the method of Schairer and Bowen (1955); in fluor-pargasites, Na was added as NaF. Cr, Ga, Sc, and In were added as oxides, dried at 400°C. End-member pargasite was also prepared as a gel after the method of Hamilton and Henderson (1968) using Na_2CO_3, $CaCO_3$, Al metal, Mg metal, and $SiO_4(C_2H_5)_4$.

Conventional or TZM-alloy cold-seal pressure vessels heated in horizontal, split-tube furnaces were used for hydroxy-pargasite syntheses. About 30 to 90 mg of mix corresponding to the appropriate anhydrous pargasitic amphibole composition plus 5 to 20 wt% double-distilled and deionized water were sealed by welding into Au capsules and reacted at temperatures between 800 and 930°C under 1- to 3-kbar water pressure. Pressure vessels were quenched under pressure by a jet of cold, compressed air followed by immersion in cold water.

Fluor-pargasite charges consisted of about 20 to 40 mg of mix with the appropriate amphibole stoichiometry. These were reacted isothermally in sealed Pt capsules suspended in vertical, quenching furnaces. Runs were quenched by dropping the capsule into a container of cold water below the furnace. Fluor-pargasite syntheses were also attempted at linear cooling rates of 1 to 2°C h^{-1}.

Capsules were weighed before and after runs to check for weight changes that would indicate capsule leaks. The capsules were then examined under a binocular microscope for external signs of leakage, especially if postrun and prerun weights were not similar. After opening, products were checked for contamination, signs of reaction with capsule material, texture, and grain size. A small portion of the product was crushed and mounted on a glass slide for viewing at higher power with a polarizing microscope.

X-ray powder diffraction

X-ray powder diffractograms were routinely taken for all run products at a scanning speed of (30°2θ min^{-1}). These allowed rapid evaluation of the amphibole yield and of the nature and approximate concentrations of nonamphibole phases. Subsequently, all runs with high yields of amphibole were scanned at 0.6°2θ min^{-1} to obtain accurate d spacings for cell-dimension measurement and identification of nonamphibole phases.

Powder diffractograms were obtained on a Philips Automated Powder Diffractometer System PW1710 using monochromatized Cu radiation (Cu$K\alpha$, wavelength = 1.5418 Å). The finely ground amphibole run product and a small amount of BaF_2 were blended thoroughly by grinding under alcohol. The mixture was spread on a glass slide with alcohol to form a thin smear. The BaF_2 [a = 6.19860(5) Å] was calibrated against Si [NBS Standard Reference Material 640a, a = 5.43083(4) Å]. Amphibole peaks were indexed by comparison with published patterns of amphiboles of known structure and composition. Only those reflections that could be unambiguously indexed and did not overlap significantly with neighboring peaks were used in cell-dimension calculations. These requirements restricted usable amphibole reflections to 10 to 12, between 9° and 45°2θ. Cell dimensions were refined using the program of Appleman and Evans (1973).

Scanning-electron microscopy

Scanning-electron micrographs of high-yield run products such as scandium-fluor-pargasite show no trace of extraneous phases (Fig. 1a); however, layer silicates are readily visible (Fig. 1b) in scanning-electron micrographs of the run products (scandium-fluor-eckermannite; Raudsepp et al., unpub. ms.) but were not observed optically or in the X-ray powder-diffraction pattern. Semiquantitative energy-dispersive spectroscopic capability would have been invaluable in the identification of these phases.

Infrared spectroscopy

Powdered samples were prepared by grinding about 10 mg of amphibole by hand in an alumina mortar with ethanol until the grain size was generally less than 2 μm. This was achieved quickly because most of the synthetic amphiboles were initially less than 2 μm in grain size. After drying to evaporate the ethanol, 3–5 mg of amphibole was mixed with 200 mg of KBr, either by hand grinding in an alumina mortar, or in a dentist's amalgamator (Wig-L-Bug). This mixture was dried under vacuum at 125°C and was pressed in an evacuated, heated die into a 13-mm pellet.

High-resolution (2.0 cm^{-1}) infrared spectra of hydroxy-amphiboles in the fundamental O–H stretching region (3600–3800 cm^{-1}) were recorded on a Nicolet Fourier transform interferometric infrared spectrophotometer, model MX-1, equipped with a Nicolet 1280 computer for signal processing. The sample chamber was purged with dry N_2 before and during spectrum collection. Frequency measurements were calibrated internally against a He-Ne laser and are accurate to 0.01 cm^{-1} according to the manufacturer.

Rietveld method of crystal-structure refinement

Specimens were ground with ethanol in an alumina mortar for at least 5 min and loaded either into an Al holder with a glass insert to support the powder, or into a HF-etched depression in a glass slide. The slurry was worked with a probe so that it was evenly distributed and dried with its surface precisely flush with the top of the holder. Grain size was generally less than 5 μm with some grains up to 20 μm long. Although most of these amphiboles crystallized with prismatic to acicular habits, preferred orientation was apparently not severe because of the extremely fine grain size, and special precautions were not taken to eliminate it during sample preparation. Attempts by other workers (e.g., Young and Wiles, 1981) to minimize preferred orientation by mixing the specimen with an equal amount of

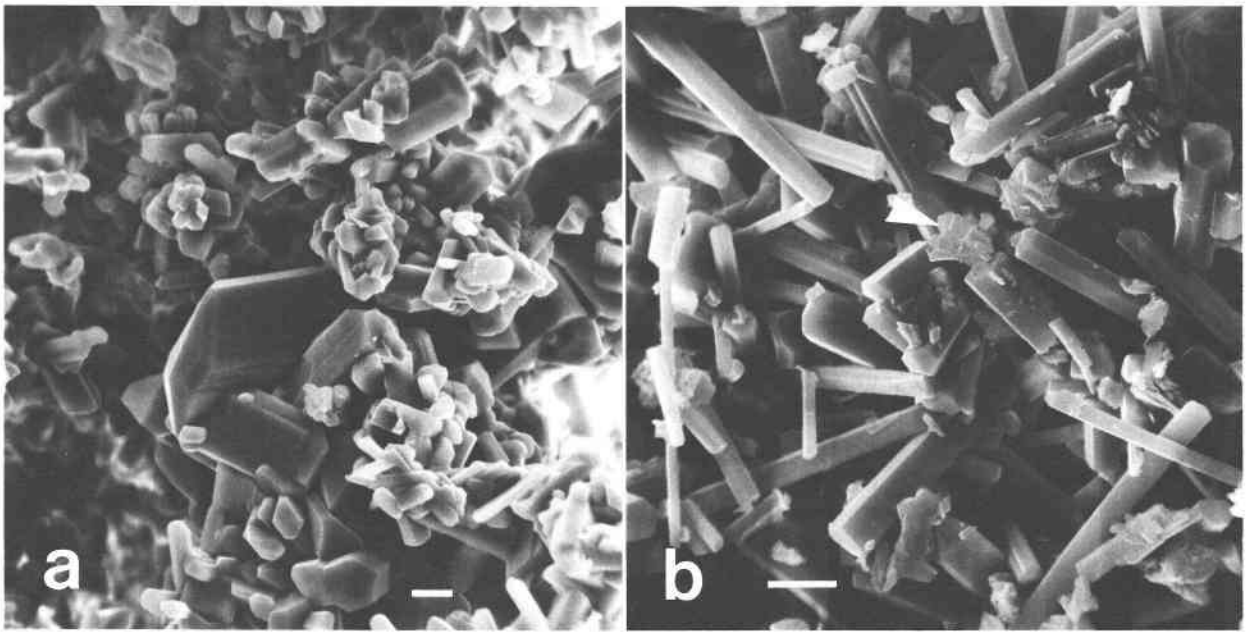

Fig. 1. Scanning-electron micrographs: (a) scandium-fluor-pargasite; (b) scandium-fluor-eckermannite (Raudsepp et al., unpub. ms.). Arrow points to layer-silicate crystals. Scale bar represents 1 μm.

inert filler (ground glass) did not significantly improve refinements.

X-ray intensity data were collected on a Philips automated diffraction system PW1710 equipped with a graphite-crystal monochromator for Cu$K\alpha$ radiation. Beam divergence was controlled with an automatic divergence slit so that a constant area (approximately 1.9 cm^2) of the specimen was irradiated throughout the scanning range. Intensities were measured at 0.02°2θ steps with counting times of either 8 or 16 s per step; scanning ranges were between 8° and 73°2θ.

Structures were refined with a slightly modified version of the program DBW 2.9 (Wiles and Young, 1981) using the modified Lorentzian peak-shape function (mod2). Refinements were done in three stages. First, the scale factor, cell parameters, and zero-point were refined with atomic positions, site occupancies, and isotropic temperature factors for individual atoms fixed at estimated values approximately correct for amphiboles. In this stage, a background model based on inspection was used; other profile parameters were estimated, either from the intensity data or from published work, and were not refined. In the second stage, the half-width parameters, peak-asymmetry parameter, and preferred-orientation parameter were included in the refinement. In addition, the background was refined as a second-order polynomial function in 2θ. Because most of the amphibole diffraction pattern above about 26°2θ consists entirely of severely overlapped peaks, background modeling was difficult. Attempts to model the background by extrapolation between areas of low intensity between peaks failed above 26°2θ. In the third stage, the remaining structural parameters were added to the refinement, and the background model function was expanded to the third order. Background refinements at higher orders failed to converge. Parameter shifts in the final cycle of refinement were generally less than 0.1 to 0.2 sigma. Best refinement results (lowest R factors) were obtained by refining an overall "isotropic temperature factor" as an approximate absorption-extinction correction. Complete refinement of a typical amphibole structure requires the simultaneous refinement of 45 to 50 parameters. In order to decrease computing time, the refinements were performed at 0.04°2θ steps rather than at the collected interval of 0.02°. The results were essentially identical; standard errors were slightly higher at the larger step interval.

MAS NMR

MAS NMR spectra were obtained on powdered minerals using a magic-angle spinning probe (Fyfe et al., 1982) and Delrin rotors on Brucker WH-400 and CXP-200 multinuclear Fourier transform NMR spectrometers equipped with 9.4- and 4.7-T superconducting magnets, respectively. The samples were spun at approximately 3500 Hz at an angle of 54.7° to the magnetic field.

^{29}Si MAS NMR spectra were recorded at a frequency of 79.46 MHz on the WH-400 spectrometer with 8192 data points using a spectral width of 25 000 Hz and 30° pulses with a 5-s delay between pulses. Chemical shifts are reported with reference to tetramethylsilane (TMS). ^{29}Si chemical shifts were calculated from the semi-empirical formula of Janes and Oldfield (1985) that uses group electronegativities of adjacent cations and takes into consideration variation in mean Si–O–Si angles.

^{27}Al MAS NMR spectra were recorded at 104.23 MHz on the WH-400 spectrometer with 30° pulses, a spectral width of 62 500 Hz and 0.3-s relaxation delay between pulses. Chemical shifts are reported in parts per million with reference to saturated aqueous $[Al(H_2O)_6]^{3+}(ClO_4)_3^-$. The broad ^{27}Al resonances are accurate to within ±0.5 ppm.

^{19}F MAS NMR spectra were recorded at a frequency of 188.15 MHz on the CXP-200 spectrometer with 8192 data points using a spectral width of 100 000 Hz and 5-s delay between pulses. Chemical shifts were determined using C_6F_6 (−162.9 ppm) as a secondary standard and are reported in ppm to low field of $CFCl_3$.

TABLE 1. Synthesis conditions and products

Run no.	T (°C)	P (bar)	t (h)	Products
				$NaCa_2Mg_4AlSi_6Al_2O_{22}(OH)_2$
GPA-A2a	930	1000	65	>95% cam + gh + cpx + fo + ne + spl?
PA-A2	840	1000	384	>95% cam + cpx + fo + pl + ne + spl?
PA-A2A	500	1000	891	>95% cam + cpx + fo + pl + ne + spl? (PA-A2 annealed)
PA-A8	840	1000	384	>95% cam + cpx + fo + pl + ne + gh
PA-A8A	590	1000	891	>95% cam + cpx + fo + pl + ne + gh (PA-A8 annealed)
PA-A10	801	1000	1126	>95% cam + cpx + fo + pl + ne + spl?
				$NaCa_2Mg_4CrSi_6Al_2O_{22}(OH)_2$
CrPA-A3	905	3000	45	80% cam + cpx + esk + spl + fo + pl + ne
CrPA-A4	846	1000	70	80% cam + esk + cpx + pl + fo + spl + ne + ly
CrPA-A5	831	2100	73	80% cam + esk + cpx + pl + fo + spl + ne + ly
				$NaCa_2Mg_4GaSi_6Al_2O_{22}(OH)_2$
GaPA-A1	758	1000	49	30% cam + cpx + pl + fo + ne + ly
GaPA-A2	846	1000	70	90% cam + cpx + pl + fo + ne + ly
GaPA-A3	817	2100	73	90% cam + cpx + fo + pl? + ne? + ly?
				$NaCa_2Mg_4ScSi_6Al_2O_{22}(OH)_2$
ScPA-A5	834	2000	70	90% cam + cpx + Sc_2O_3 + fo + ne + pl
ScPA-A6	830	2000	70	90% cam + cpx + Sc_2O_3 + fo + ne + pl
				$NaCa_2Mg_4InSi_6Al_2O_{22}(OH)_2$
InPA-A4	838	2000	73	90% cam + cpx + gh + fo + In_2O_3
				$NaCa_2Mg_4AlS_6Al_2O_{22}F_2$
FPA-NMR	1000	1	63	>90% cam + cpx + pl + spl + ne + fo
FPA-BUL	1000	1	48	>90% cam + cpx + pl + spl + ne + fo
FPA-B4	1193–799	1	308	>90% cam + pl + fl + cpx + spl + fo + ne
FPA-B5	938	1	120	>90% cam + cpx + pl + spl + ne + fo
				$NaCa_2Mg_4CrSi_6Al_2O_{22}F_2$
FCrPA-A1	1006	1	71	80% cam + mchr + pl + cpx + fo
FCrPA-A3	1000	1	90	80% cam + mchr + pl + cpx + fo
				$NaCa_2Mg_4GaSi_6Al_2O_{22}F_2$
FGaPA-A1	1006	1	71	85% cam + pl + fo + cpx
FGaPA-A2	1273–844	1	382	85% cam + fo + pl + cpx + fl + gl
FGaPA-A3	1000	1	90	85% cam + pl + fo + cpx
				$NaCa_2Mg_4ScSi_6Al_2O_{22}F_2$
FScPA-A1	1006	1	71	>95% cam + cpx + fo + ne?
FScPA-A3	1073	1	75	>95% cam + cpx + fo + ne?

Note: Abbreviations: cam = clinoamphibole; fo = forsterite; ly = layer silicate; esk = eskolaite; ne = nepheline; cpx = clinopyroxene; gh = gehlenite; pl = plagioclase; spl = spinel; gl = glass; mchr = magnesio-chromite; fl = fluorite.

EXPERIMENTAL RESULTS

Synthesis products

Synthesis conditions and products for typical pargasitic amphiboles grown in this study are given in Table 1. Only those phases that could be unambiguously identified from powder X-ray patterns, or rarely, optically, are listed. Typical amphiboles grown in this study formed blocky to prismatic crystals 1 to 20 μm wide and up to 40 μm long. Cr-bearing varieties were pale green and slightly pleochroic; indium-pargasite was very pale yellow and faintly pleochroic; all others were clear and colorless. Cell dimensions for pargasites from selected runs are given in Table 2, and full run descriptions are given in Table 3.[1]

[1] To obtain a copy of Table 3, order Document AM-87-335 from the Business Office, Mineralogical Society of America, 1625 I Street, N.W., Suite 414, Washington, D.C. 20006, U.S.A. Please remit $5.00 in advance for the microfiche.

Infrared spectroscopy

In the 3800–3300-cm^{-1} region, high-resolution infrared spectra of amphiboles exhibit fine structure that is sensitive to the cation occupancies of the M(1) and M(3) sites (Hawthorne, 1983a, 1983b). In binary solid solutions, there are eight possible ways of distributing two different cations over the three M sites coordinating each hydroxyl. In amphiboles, however, the three M sites coordinating the hydroxyl are in a pseudotrigonal arrangement that introduces an accidental degeneracy to some bands and reduces the number of resolvable bands to four. In end members, 2M(1) + M(3) configurations around each hydroxyl are identical, and a single, sharp hydroxyl-stretching band results (Fig. 2). Figure 2 shows typical natural amphibole spectra collected under the same experimental conditions as the synthetic amphibole spectra. Note the sharp, narrow peaks with band widths between 6 and 9 cm^{-1}, typical values for natural amphibole

TABLE 2. Cell dimensions of synthetic pargasitic amphiboles

Run no.	a (Å)	b (Å)	c (Å)	β (°)	V (Å^3)
		$NaCa_2Mg_4AlSi_6Al_2O_{22}(OH)_2$			
GPA-A2A	9.904(3)	17.941(5)	5.281(2)	105.54(3)	904.0(3)
PA-A8A	9.907(3)	17.929(6)	5.282(2)	105.51(2)	904.0(3)
PA-A2A	9.894(2)	17.948(5)	5.280(1)	105.50(2)	903.5(3)
PA-A10	9.897(2)	17.946(4)	5.284(1)	105.51(2)	904.4(2)
		$NaCa_2Mg_4CrSi_6Al_2O_{22}(OH)_2$			
CrPA-A3	9.914(2)	17.993(4)	5.285(1)	105.44(2)	908.7(2)
CrPA-A4	9.917(3)	17.998(6)	5.287(2)	105.41(2)	909.8(3)
CrPA-A5	9.909(2)	17.989(5)	5.285(2)	105.42(2)	908.2(3)
		$NaCa_2Mg_4GaSi_6Al_2O_{22}(OH)_2$			
GaPA-A1	9.849(2)	17.953(4)	5.297(1)	105.17(2)	903.9(2)
GaPA-A2	9.923(3)	17.973(5)	5.292(1)	105.49(2)	909.7(3)
GaPA-A3	9.910(4)	17.976(7)	5.289(2)	105.54(3)	907.9(2)
		$NaCa_2Mg_4ScSi_6Al_2O_{22}(OH)_2$			
ScPA-A5	9.942(3)	18.101(5)	5.297(1)	105.37(2)	919.2(3)
ScPA-A6	9.944(2)	18.096(5)	5.298(1)	105.39(2)	919.2(3)
ScPA-A5*	9.9405(7)	18.094(1)	5.2986(4)	105.364(5)	918.97
		$NaCa_2Mg_4InSi_6Al_2O_{22}(OH)_2$			
InPA-A4	9.937(3)	18.030(4)	5.289(2)	105.54(2)	912.9(3)
		Fluor-pargasite			
		$NaCa_2Mg_4AlSi_6Al_2O_{22}F_2$			
FPANMR	9.830(4)	17.919(6)	5.294(2)	105.16(3)	900.0(3)
FPA-BUL	9.827(3)	17.927(7)	5.293(2)	105.19(3)	899.8(4)
FPA-B4	9.818(3)	17.929(7)	5.295(2)	105.27(4)	899.2(4)
FPA-B5	9.820(3)	17.931(5)	5.293(2)	105.20(3)	899.4(3)
FPA-BUL*	9.8277(7)	17.930(1)	5.2931(4)	105.168(4)	900.21
		$NaCa_2Mg_4CrSi_6Al_2O_{22}F_2$			
FCrPA-A1	9.834(3)	17.971(5)	5.286(1)	105.07(2)	902.1(3)
FCrPA-A3	9.845(8)	18.005(13)	5.284(4)	105.06(6)	904.4(7)
FCrPA-A3*	9.8402(5)	17.9800(9)	5.2914(3)	105.108(3)	903.83
		$NaCa_2Mg_4GaSi_6Al_2O_{22}F_2$			
FGaPA-A1	9.846(2)	17.951(4)	5.296(1)	105.16(2)	903.5(2)
FGaPA-A2	9.852(3)	17.945(4)	5.299(1)	105.25(2)	903.9(2)
FGaPA-A3*	9.8600(5)	17.9685(9)	5.3027(3)	105.198(3)	906.62
		$NaCa_2Mg_4ScSi_6Al_2O_{22}F_2$			
FScPA-A1	9.881(2)	18.145(4)	5.317(1)	105.17(2)	920.1(2)
FScPA-A3*	9.8852(4)	18.1574(7)	5.3186(2)	105.213(2)	921.18

* Determined by Rietveld structure refinement.

spectra (Strens, 1974). Of particular interest is the peak shape of the single MgMgMg stretching band in the tremolite spectrum (Fig. 2a). The shape corresponds to that of a markedly skewed Gaussian distribution. Figure 2 shows a typical natural actinolite spectrum with Mg and Fe^{2+} as the predominant octahedral cations. Infrared spectra of synthetic pargasites with M^{3+} = Al, Cr, Ga, and Sc are presented in Figure 3. For the ordered case, in which the M(2) site occupancy is $0.5Mg + 0.5M^{3+}$ and the M(1,3) sites are occupied solely by Mg, the spectrum should consist of a single band corresponding to the MgMgMg configuration. However, the spectrum of pargasite (M^{3+} = Al) consists of two major bands at 3709 and 3676 cm^{-1}, and a weak shoulder at about 3645 cm^{-1}. Because the sample was from a high-yield run and therefore close to the nominal composition, the two major bands were assigned to the MgMgMg and MgMgAl configurations, respectively; the weak band is probably due to minor A-site vacancies.

Band widths (Fig. 3) are about 25 to 33 cm^{-1}, which are considerably larger than typical values of about 6 cm^{-1} for natural amphibole spectra (Fig. 2). The origin of the large band width in synthetic amphiboles is not clear. It is tempting to ascribe it to poor crystal quality (high mosaicity) inducing positional disorder that resulted in a minor shift of the principal stretching band; however, the powder-diffraction patterns suggest a high degree of crystallinity. Additionally, the degree of local disorder in intermediate natural amphibole solutions did not cause broadening of infrared peaks on this sort of scale (Fig. 2b), and consequently it is difficult to envision local disorder as the cause of broadening in scandium-pargasite, in which the Mg and Sc are of fairly similar size, and in which the amphibole seemed to have good crystallinity. Thus, we cannot propose a convincing reason for the wide peaks in the infrared spectra of these amphiboles.

The frequency shift of the MgMgAl band relative to the MgMgMg band is -33 cm^{-1}. Semet (1973) also recorded the frequency shift of the MgMgAl band in the synthetic pargasite spectrum as -33 cm^{-1}. Strens (1974) showed that the frequency shifts of individual bands (in reciprocal centimeters) are a function of the electronega-

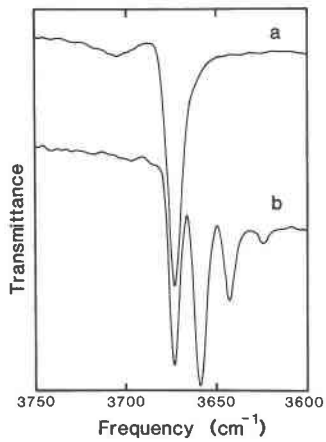

Fig. 2. Typical infrared spectra of (a) natural tremolite and (b) natural actinolite.

tivities of the bonded cations according to the approximate relationship

$$\Delta v = 35n(X_{Mg} - X_s),$$

where $0 < n < 3$ is the number of Mg ions replaced in any one $Mg_3(OH)_2$ cluster, and X_{Mg} and X_s are the Allred-Rochow electronegativities of Mg and the substituent cation, respectively. This gives a frequency shift of -9 cm^{-1} for the MgMgAl band relative to MgMgMg, which is significantly different from the observed shift of -33 cm^{-1}. Clearly, the magnitude of the frequency shift is not a simple function of electronegativity. The frequency shifts given by Strens (1974) were determined mainly from configurations involving Mg and divalent cations, so presumably the shifts observed for trivalent cations cannot be adequately described using this equation owing to the different formal charge of the cations involved.

Infrared spectra of chromium-pargasite and gallium-pargasite (from this study) and magnesio-hastingsite (Semet, 1973) all have shoulders near 3676 cm^{-1} (Fig. 4) corresponding to the MgMgAl configuration in end-member pargasite (Fig. 3). These spectra suggest that synthetic pargasites (M^{3+} = Cr, Ga, or Sc) and magnesio-hastingsite (M^{3+} = Fe^{3+}) are not of the nominal compositions but contain minor octahedral Al. This discrepancy between the nominal composition and the composition of the synthetic amphiboles is particularly evident in the spectrum of chromium-pargasite (M^{3+} = Cr), which consists of major bands at 3710 and 3659 cm^{-1} and a weak shoulder at 3674 cm^{-1} (Fig. 3). The two major bands were assigned to MgMgMg and MgMgCr configurations; the shoulder at 3674 cm^{-1} is probably due to the MgMgAl configuration. The spectrum of gallium-pargasite (M^{3+} = Ga) is similar. Bands at 3706, 3676, and 3665 cm^{-1} were assigned to the MgMgMg, MgMgAl, and MgMgGa configurations, respectively. Both chromium- and gallium-pargasite spectra exhibit poorly resolved fine structure other than the three principal bands. These may be due to inadequate resolution or perhaps to the presence

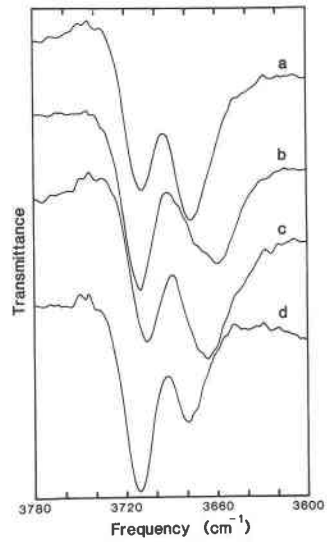

Fig. 3. Infrared spectra of synthetic pargasites: (a) pargasite; (b) chromium-pargasite; (c) gallium-pargasite; (d) scandium-pargasite.

of minor layer-silicate impurities. In contrast to chromium- and gallium-pargasites, the scandium-pargasite (M^{3+} = Sc) spectrum is straightforward. The three major bands at 3711, 3679, and 3673 cm^{-1} were assigned to the MgMgMg, MgMgAl, and MgMgSc configurations, respectively.

Rietveld crystal-structure refinement

The Rietveld method (Rietveld, 1967, 1969) uses the whole powder-diffraction pattern to characterize the

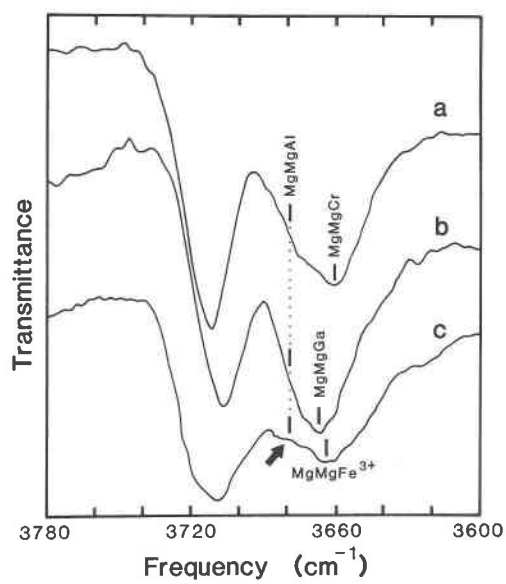

Fig. 4. Infrared spectra of synthetic pargasites and magnesio-hastingsite. Arrow points to MgMgAl bands additional to MgMgCr, MgMgGa, and MgMgFe^{3+} bands. (a) Chromium-pargasite; (b) gallium-pargasite; (c) magnesio-hastingsite (from Semet, 1973).

TABLE 4. Atomic positions for synthetic pargasitic amphiboles

		ScPA-A5	FPA-BUL	FCrPA-A3	FGaPA-A3	FScPA-A3
O(1)	x	0.117(2)	0.119(1)	0.113(1)	0.118(1)	0.1108(9)
	y	0.0935(8)	0.0868(6)	0.0876(6)	0.0896(5)	0.0864(4)
	z	0.233(2)	0.216(2)	0.212(2)	0.221(2)	0.219(2)
O(2)	x	0.108(2)	0.116(1)	0.114(1)	0.106(1)	0.1138(9)
	y	0.1741(6)	0.1676(6)	0.1703(5)	0.1703(5)	0.1709(4)
	z	0.712(2)	0.740(2)	0.740(2)	0.730(2)	0.724(1)
O(3)	x	0.109(2)	0.106(1)	0.100(1)	0.101(1)	0.1008(9)
	y	0	0	0	0	0
	z	0.713(5)	0.711(4)	0.714(3)	0.709(3)	0.711(2)
O(4)	x	0.352(1)	0.366(2)	0.359(1)	0.359(1)	0.3598(8)
	y	0.2495(6)	0.2522(6)	0.2498(5)	0.2487(5)	0.2468(4)
	z	0.770(4)	0.782(3)	0.792(2)	0.790(2)	0.788(2)
O(5)	x	0.354(1)	0.357(1)	0.363(1)	0.350(1)	0.3535(9)
	y	0.1401(5)	0.1380(5)	0.1379(4)	0.1377(4)	0.1388(3)
	z	0.119(3)	0.126(2)	0.134(2)	0.116(2)	0.122(2)
O(6)	x	0.344(2)	0.341(1)	0.342(1)	0.346(1)	0.3447(9)
	y	0.1091(6)	0.1091(5)	0.1116(4)	0.1093(4)	0.1140(3)
	z	0.638(3)	0.631(3)	0.622(3)	0.615(2)	0.620(2)
O(7)	x	0.348(2)	0.348(2)	0.356(1)	0.344(1)	0.353(1)
	y	0	0	0	0	0
	z	0.290(5)	0.286(4)	0.295(3)	0.278(3)	0.291(2)
T(1)	x	0.2824(8)	0.2821(7)	0.2817(6)	0.2844(6)	0.2838(5)
	y	0.0820(3)	0.0831(3)	0.0824(3)	0.0842(2)	0.0833(2)
	z	0.303(2)	0.309(2)	0.301(1)	0.307(1)	0.304(1)
T(2)	x	0.288(1)	0.2953(9)	0.2924(7)	0.2893(7)	0.2909(5)
	y	0.1682(3)	0.1721(3)	0.1703(3)	0.1707(2)	0.1692(2)
	z	0.811(2)	0.809(1)	0.813(1)	0.809(1)	0.8090(9)
M(1)	x	0	0	0	0	0
	y	0.0865(5)	0.0888(5)	0.0879(4)	0.0875(4)	0.0870(3)
	z	½	½	½	½	½
M(2)	x	0	0	0	0	0
	y	0.1751(4)	0.1775(5)	0.1767(4)	0.1749(4)	0.1763(3)
	z	0	0	0	0	0
M(3)	x	0	0	0	0	0
	y	0	0	0	0	0
	z	0	0	0	0	0
M(4)	x	0	0	0	0	0
	y	0.2811(3)	0.2768(3)	0.2776(3)	0.2786(3)	0.2791(2)
	z	½	½	½	½	½
A	x	0	0.024(3)	0.031(2)	0.017(3)	0.029(2)
	y	½	½	½	½	½
	z	0	0.057(1)	0.072(5)	0.068(5)	0.068(4)

Note: Isotropic temperature factors (B): O(1) = O(2) = O(3) = O(4) = 0.8; O(5) = O(6) = 1.1; O(7) = 1.2; T(1) = T(2) = 0.4; M(1) = M(2) = M(3) = 0.6; M(4) = 0.9; A = 2.3

TABLE 5. Interatomic distances (Å) for synthetic pargasitic amphiboles

	ScPA-A5	FPA-BUL	FCrPA-A3	FGaPA-A3	FScPA-A3
T(1)–O(1)	1.600	1.554	1.604	1.586	1.651
T(1)–O(5)	1.709	1.681	1.668	1.649	1.667
T(1)–O(6)	1.784	1.715	1.726	1.653	1.725
T(1)–O(7)	1.630	1.642	1.656	1.646	1.668
⟨T(1)–O⟩	1.681	1.648	1.664	1.634	1.678
T(2)–O(2)	1.728	1.705	1.694	1.745	1.690
T(2)–O(4)	1.639	1.618	1.588	1.575	1.581
T(2)–O(5)	1.671	1.738	1.758	1.686	1.706
T(2)–O(6)	1.596	1.610	1.622	1.700	1.605
⟨T(2)–O⟩	1.659	1.668	1.666	1.677	1.646
M(1)–O(1) ×2	2.061	2.129	2.109	2.110	2.072
M(1)–O(2) ×2	2.072	2.037	2.081	2.031	2.073
M(1)–O(3) ×2	2.061	2.064	2.039	2.027	2.040
⟨M(1)–O⟩	2.065	2.077	2.076	2.056	2.062
M(2)–O(1) ×2	2.072	2.149	2.101	2.088	2.133
M(2)–O(2) ×2	2.088	2.011	1.994	1.984	2.075
M(2)–O(4) ×2	2.134	1.964	2.022	2.062	2.078
⟨M(2)–O⟩	2.098	2.041	2.039	2.045	2.095
M(3)–O(1) ×4	2.230	2.097	2.081	2.146	2.085
M(3)–O(3) ×2	2.087	2.063	2.008	2.042	2.038
⟨M(3)–O⟩	2.182	2.086	2.057	2.111	2.069
M(4)–O(2) ×2	2.351	2.448	2.420	2.387	2.416
M(4)–O(4) ×2	2.374	2.296	2.380	2.379	2.368
M(4)–O(5) ×2	2.581	2.601	2.554	2.649	2.615
M(4)–O(6) ×2	2.740	2.768	2.707	2.686	2.655
⟨M(4)–O⟩	2.512	2.528	2.515	2.525	2.514

structure of a material. The structure parameters of the mineral, atomic coordinates, site occupancies, and thermal parameters, together with various experimental parameters affecting the pattern, are refined by least-squares procedures to minimize the difference between the whole calculated and observed patterns.

Structures of five pargasitic amphiboles synthesized in this study were refined with the Rietveld method. Results of the structure refinements are summarized in Tables 4 to 7. The Rietveld agreement index R_{wp} varied between 11.4 and 14.6%. A typical calculated and observed powder-diffraction pattern is given in Figure 5 for scandium-fluor-pargasite (FScPA-A3).

Cell dimensions derived from the refinements are given in Table 2. In general, they are up to an order of magnitude more precise than those derived from normal least-squares refinement of powder-diffraction data (Table 2). With the exception of gallium-fluor-pargasite, cell dimensions are identical within 2 or 3 sigma for both methods of determination for identical samples. Atomic positions are given in Table 4. Interatomic distances (Table 5) were calculated using RFINE (Finger, 1969). Individual tetrahedral bond lengths (Table 5) exhibit ranges of variation that are inconsistent with single-crystal structure data for both pargasites and alkali amphiboles. Mean tetrahedral bond lengths are better behaved and are reasonable, except for gallium-fluor-pargasite (4) in which ⟨T(2)–O⟩ is much larger than ⟨T(1)–O⟩. Variation in individual ⟨M–O⟩ with mean ionic radii of constituent octahedral cations is not consistent with trends for single-crystal structures (Hawthorne, 1983b).

In the amphibole structure, there are pseudo–glide planes ∥(010) at $y = \pm¼$, and thus the T(1) and T(2) tetrahedra are pseudosymmetrically related. The diffractions containing information on the differences between the T(1) and T(2) tetrahedra are very weak, and consequently the shifts of the atomic positions of the atoms concerned are highly correlated during least-squares refinement (Table 6). The derivative information, such as bond lengths, is thus rather imprecise. Similar effects occur in the $P2_1/c$ pyroxenes examined by Hawthorne et al. (1984), Raudsepp et al. (1984), and Raudsepp et al. (unpub. ms.). In the $P2_1/c$ pyroxenes, pseudo–C-centering results in high correlations of the tetrahedral positions

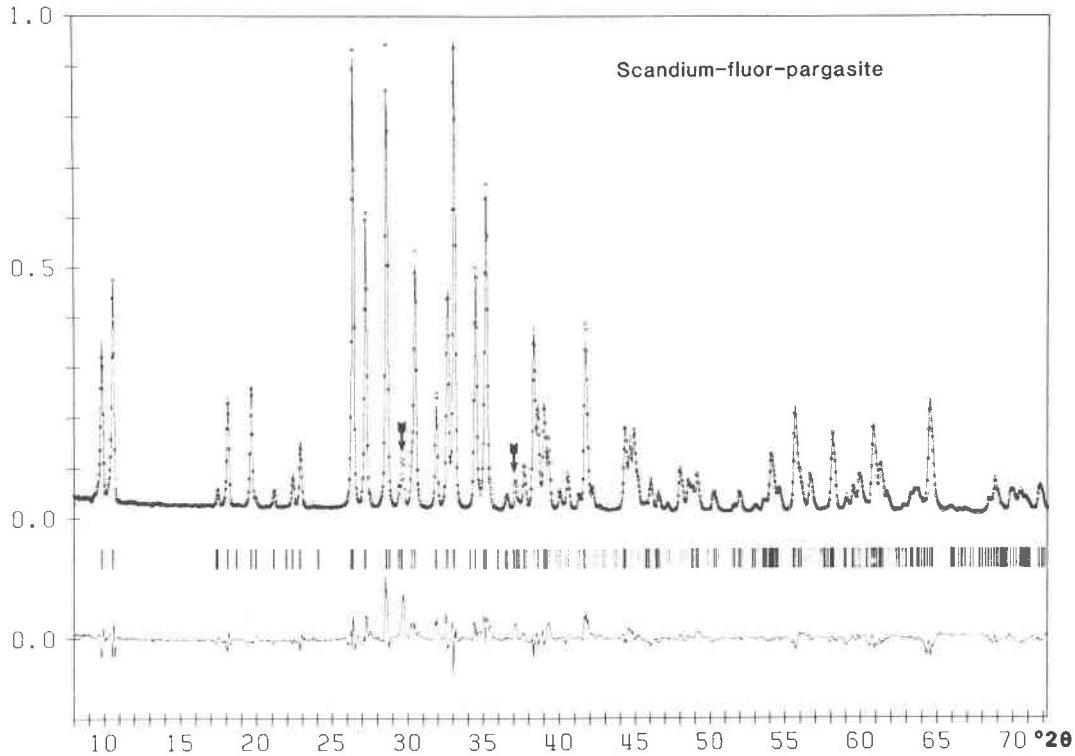

Fig. 5. Calculated and observed X-ray diffraction pattern of scandium-fluor-pargasite from Rietveld structure refinement. Open squares are the observed data, solid line is the calculated pattern, and the vertical bars below the pattern mark all possible Bragg reflections ($K\alpha_1$ and $K\alpha_2$). The residual pattern obtained by subtracting the observed and calculated patterns is shown below.

and unrealistic bond lengths; however, site occupancies determined by Rietveld refinement and Mössbauer spectroscopy are in good agreement. For structures in which such pseudosymmetry does not occur (e.g., olivine), there is good agreement between Rietveld and single-crystal data for both atomic positions and site occupancies (Raudsepp et al., unpub. ms.). This suggests that the high correlations should not affect the site occupancies given here for the amphiboles, and hence they should be fairly accurate.

Synthetic amphibole site occupancies are given in Table 7. All negative values differ from zero by less than 3 sigma and may be regarded as zero; similarly, occupancies greater than 1.0 may be set to 1.0. In general, powder structure refinements of these synthetic amphiboles were comparable with most powder refinements of other minerals (Young, 1980). Rietveld refinement is still a technique undergoing rapid development, and several aspects are currently not satisfactory:

1. The peak profile function used in the Rietveld analysis did not adequately model the observed peak shape. Difference plots (Fig. 5) show consistent sinusoidal fluc-

TABLE 6. Selected correlations from Rietveld refinement of scandium-fluor-pargasite

Atoms	x	y	z
O(4)–O(7)	−0.25	0	−0.62
O(1)–O(2)	−0.54	0.25	−0.37
O(5)–O(6)	−0.60	0.18	−0.03
T(1)–T(2)	−0.69	0.04	−0.66

TABLE 7. M(1), M(2), M(3) site occupancies of synthetic pargasitic amphiboles

		Scandium pargasite		
M(1)	Mg	1.037(22)	Sc	−0.037(22)
M(2)	Mg	0.789(20)	Sc	0.211(20)
M(3)	Mg	0.792(27)	Sc	0.208(27)
		Fluor-pargasite		
M(1)				
M(2)	(occupancies indeterminate)			
M(3)				
		Chromium-fluor-pargasite		
M(1)	Mg	0.920(10)	Cr	0.080(10)
M(2)	Mg	0.840(11)	Cr	0.160(11)
M(3)	Mg	1.061(14)	Cr	−0.061(14)
		Gallium-fluor-pargasite		
M(1)	Mg	1.002(6)	Ga	−0.002(6)
M(2)	Mg	0.900(6)	Ga	0.100(6)
M(3)	Mg	0.962(8)	Ga	0.038(8)
		Scandium-fluor-pargasite		
M(1)	Mg	0.922(11)	Sc	0.078(11)
M(2)	Mg	0.597(12)	Sc	0.403(12)
M(3)	Mg	1.005(15)	Sc	−0.005(15)

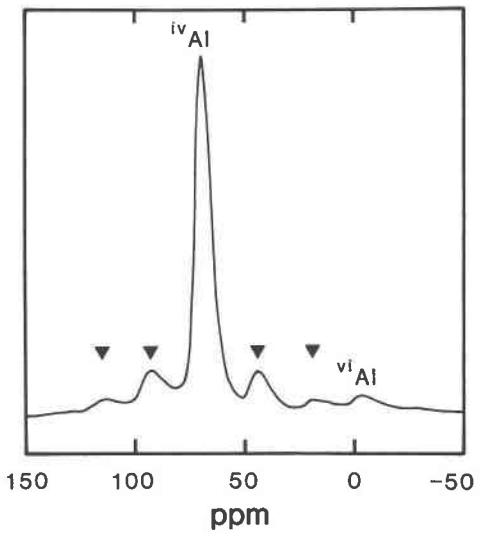

Fig. 6. ^{27}Al MAS NMR spectrum of synthetic scandium-fluor-pargasite; ▼ denotes spinning sidebands.

tuations that reflect inadequate fits at the peak base. These are best observed for the (020) and (110) peaks between 9.5° and 10.6°2θ.

2. The single refinable asymmetry parameter did not adequately model peak asymmetry over the entire 2θ range. Best results (lowest R_{wp} values) were obtained by refining the asymmetry parameter only below about 32°2θ; refining this parameter for the whole patern gave higher R values.

3. All of the samples contained from 1 to 10% extraneous phases that contributed to the overall pattern. Peaks due to phases other than amphibole are marked by arrows in Figure 5 and listed in Table 1. The refinement program allows regions of extraneous intensity to be excluded, but extra intensity under amphibole peaks could not be excluded in this way; this raises the R factors significantly.

Conversely, the residual pattern that remains (Fig. 5) after the observed diffraction pattern is subtracted from the calculated pattern is valuable because it comprises the diffraction patterns of phases other than amphibole in the run product. In the whole pattern, the scattering contributions of these phases are partly or completely masked by the intense amphibole pattern; this may lead to the false assumption that the amphibole yield is near 100%. With the current profile function, the interpretation of this residual pattern is not straightfoward because the diffraction patterns of extraneous phases are mixed with residual intensity derived from inadequate peak-shape models. However, this situation will improve when more adequate peak-shape algorithms become available.

Use of the Rietveld method ensures that the amphibole pattern is correctly indexed and that non-amphibole peaks are not indexed as amphibole peaks. This is of more importance than one would initially think, as several published synthetic-amphibole diffraction patterns have incorrect indexing and wrong cell dimensions as a result of the presence of non-amphibole peaks.

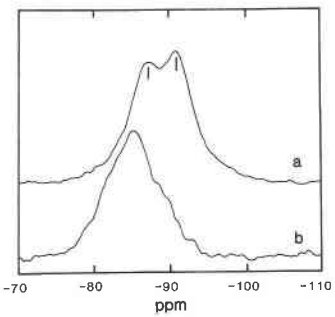

Fig. 7. ^{29}Si MAS NMR spectra: (a) natural tremolite; (b) scandium-fluor-pargasite.

MAS NMR

The ^{27}Al spectrum of scandium-fluor-pargasite is shown in Figure 6. The ^{27}Al chemical shifts are known to be sensitive to the coordination of Al (Mueller et al., 1981); shifts around 0 ppm correspond to octahedrally coordinated Al, and shifts around 70 ppm correspond to tetrahedrally coordinated Al. The major peak in Figure 6 is at 68.5 ppm, corresponding to tetrahedrally coordinated Al as expected for a pargasitic amphibole. This central peak is flanked by two pairs of spinning sidebands (marked as such in Fig. 6) and an additional very small peak at −3.8 ppm. The latter corresponds to octahedrally coordinated Al, and the relative intensities of the two peaks indicate that it represents about 4% of the total Al. Note that the infrared spectrum of scandium-pargasite (the hydroxy analogue) also indicates the presence of a small amount of octahedrally coordinated Al (Fig. 3).

The ^{29}Si spectrum of a natural tremolite is shown in Figure 7a. There are two resolved peaks of approximately equal intensity at −87.2 and −90.2 ppm, respectively, corresponding to Si at the T(2) and T(1) sites in the structure; a similar spectrum is given by Smith et al. (1983). The peak at −87.2 ppm is assigned to the T(2) site with two adjacent silicate tetrahedra, and the peak at −90.2 ppm is assigned to the T(1) site with three adjacent tetrahedra, in accordance with the shift to high field with condensation (Lippmaa et al., 1980). This peak assignment is corroborated by the calculations of Janes and Oldfield (1985) of the chemical shift in tremolite (Table 8). The differences between our measured values and Janes and Oldfield's calculated and measured values of chemical shift are consistent with variations in composition and order in the two natural samples.

The ^{29}Si spectrum of scandium-fluor-pargasite is shown in Figure 7b. There is a broad resonance centered at about −85 ppm apparently consisting of several overlapping peaks. This spectrum was resolved into a series of Lorentzian peaks by the method of least-squares, using the constraint that the half-widths (full-width at half-maximum) of all peaks be equal. The minimum possible number of component peaks in the spectrum is four, and so-

TABLE 8. Observed and calculated ^{29}Si MAS NMR chemical shift for amphiboles

Site	Calculated*	Measured	
	Tremolite		
T(1) (3Si)	−93.8	−92.2†	−90.2
T(2) (2Si)	−83.9	−87.8†	−87.2
	Fluor-scandium-pargasite		
T(1) (3Si)	−90.0		
T(1) (2Si1Al)	−86.8		
T(1) (1Si2Al)	−82.7		
T(2) (2Si)	−82.5		
T(1) (3Al)	−79.3		
T(2) (1Si1Al)	−78.4		
T(2) (2Al)	−74.3		

* From the relationship of Janes and Oldfield (1985); shifts in parts per million relative to TMS.

† Janes and Oldfield (1985), Table 11 (data from Mägi et al., 1984).

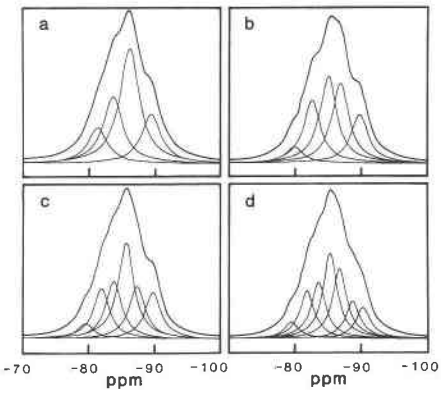

Fig. 8. (a) Four, (b) five, (c) six, and (d) seven peak fits to the ^{29}Si MAS NMR spectrum of pargasite. Calculated spectrum is shown; experimental envelope shown in Fig. 7b.

lutions were calculated for four, five, six, and seven peaks. The calculated spectra are shown in Figure 8 and may be compared with the observed spectrum in Figure 7b. The positions and calculated intensities of the component peaks in these spectra are listed in Table 9.

The local arrangements of atoms around the T(1) and T(2) positions are shown in Figure 9. Using the labeling of Figure 9, the possible next-nearest-neighbor arrangements are shown in Table 10; there are eight possible arrangements for T(1) and four possible arrangements for T(2), labeled 1 to 12, respectively. Peaks resulting from arrangements 2, 3, and 5 will closely overlap, as will those for arrangements 4, 6, and 7 and arrangements 10 and 11, reducing the number of possible resolved peaks to seven. The number of peaks could be further reduced because of the energetic unfavorability of certain arrangements or by accidental overlap. The resolution of the spectrum is not really sufficient to a priori decide on the number of peaks that actually occur. However, we may consider possible arrangement models, and their compatibility with the observed spectrum may allow us to accept or reject certain of these arrangements. Therefore, with regard to Al-Si ordering over the tetrahedral sites, we may recognize in general four possible models:

Model 1. All Al ordered at T(1), no Al-O-Al linkages allowed. This model would produce four peaks, numbers 5, 9, (10 + 11), and 12; as the amount of Si at T(1) would be half that at T(2), the intensity of peak 5 would be one-third of the total intensity, assuming that the transition probability is the same for each arrangement.

Model 2. All Al ordered at T(1), Al-O-Al linkages allowed. This model would produce five peaks, numbers 1, 5, 9, (10 + 11), and 12; the sum of the intensities of peaks 1 and 5 would be one-third of the total intensity.

Model 3. Al disordered over T(1) and T(2), no Al-O-Al linkages allowed. This model would produce six peaks, numbers 5, (6 + 7), 8, 9, (10 + 11), and 12; the sum of the intensities of 5 + (6 + 7) + 8 would be half the total intensity for complete Al disorder.

Model 4. Al disordered over T(1) and T(2), Al-O-Al linkages allowed. All seven peaks would occur, with the sum of the intensities of 1 + (2 + 3 + 5) + (4 + 6 + 7) equal to half of the total intensity for complete Al disorder.

First, we consider the case for which there is no accidental overlap of peaks, and the high- to low-field sequence of peaks is as calculated in Table 8. Comparison of the observed and ideal intensities for the various number of peaks in each of the above models is shown in Table 9. By far the best agreement occurs for model 3 in which Al is disordered over T(1) and T(2) (but there are no Al–O–Al linkages) and six peaks result. Next, we consider the possibility of accidental positional degeneracy. Examination of Table 8 shows that arrangements (4 +

TABLE 9. Peak fits to the ^{29}Si MAS NMR spectrum of scandium-fluor-pargasite

No. of peaks fitted	Peak position (ppm)	Peak intensity (arbitrary units)	Intensity observed (% of total)	Ideal model value (%)	Difference |obs. − ideal| (%)
4	−89.9	17339	19	33	14
	−86.1	40328	—	—	—
	−83.0	23564	—	—	—
	−80.2	12505	—	—	—
5	−90.3	15103	44	33	11
	−86.8	24865			
	−84.6	26993	—	—	—
	−81.6	19531	—	—	—
	−78.7	4991	—	—	—
6	−90.5	13217	49	50	1
	−87.7	14891			
	−85.6	27222	—	—	—
	−83.3	16248			
	−81.2	14243	—	—	—
	−78.3	4190	—	—	—
7	−91.1	8069	40	50	10
	−89.3	9871			
	−86.8	17956			
	−85.1	21856	—	—	—
	−83.1	14481	—	—	—
	−81.0	12341	—	—	—
	−78.2	4228	—	—	—

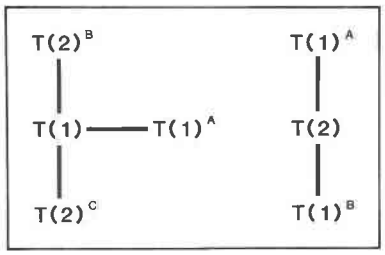

Fig. 9. Next-nearest-neighbor (tetrahedral site) arrangements about the T(1) and T(2) sites in clinoamphiboles.

6 + 7) [T(1) = 1Si2Al] and 9 [T(2) = 2Si] have approximately the same calculated position and quite possibly could result in overlapping peaks. This being the case, models 1 and 2 would contain the same number of peaks, as they do not have any arrangements involving peaks 4, 6, and/or 7. On the other hand, models 3 and 4 do have both peak (4 + 6 + 7) and peak 9, and overlap would reduce the number of *resolved* peaks to five and six, respectively. For model 2, the intensity of the first two resolved peaks [5 + (6 + 7 + 9)] is ideally 50% + intensity of peak 9; thus the ideal intensity is significantly greater than 50%; the observed value (Table 9, five-peak fit) is 44%, and the deviation is thus significantly greater than 6%. For model 4, the above-mentioned overlap results in six peaks, and the ideal intensity of the first three peaks must be significantly greater than 50%; the observed value is 60%, so model 4 also seems possible.

Summarizing the above results, the ^{29}Si MAS NMR spectrum of scandium-fluor-pargasite shows much better agreement for ordering models involving Al disorder at the T(1) and T(2) sites; in addition, the agreement is better for a model involving no ^{IV}Al–O–^{IV}Al linkages.

^{19}F MAS NMR spectra of tremolite (Fig. 10a) and fluor-scandium-pargasite (Fig. 10b) consist of one very broad peak at −171.7 and −169.6 ppm, respectively, with multiple spinning sidebands. The F is in a more asymmetric environment in the pargasite than in tremolite as shown by the larger intensity of the spinning sidebands in the pargasite spectrum. This is probably due to the presence

TABLE 10. Possible next-nearest-neighbor arrangements in pargasite

Arrangement	A	B	C
		T(1) site	
1	Si	Si	Si
2	Si	Al	Si
3	Si	Si	Al
4	Si	Al	Al
5	Al	Si	Si
6	Al	Al	Si
7	Al	Si	Al
8	Al	Al	Al
		T(2) site	
9	Si	Si	
10	Si	Al	
11	Al	Si	
12	Al	Al	

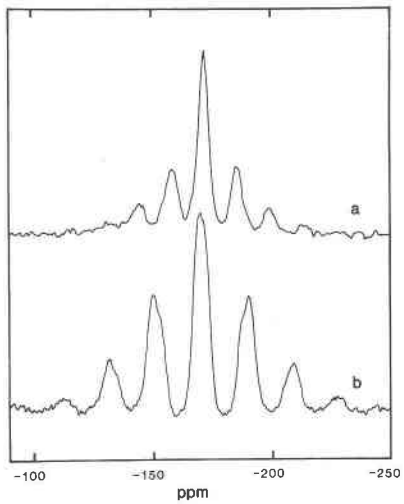

Fig. 10. ^{19}F MAS NMR spectra of (a) tremolite; (b) fluor-scandium-pargasite.

of Sc at some M sites and positionally disordered Na at the A(2) and A(m) sites, locally destroying the mirror symmetry at the O(3) site. The principal peak in the pargasite spectrum has some structure at the top; the shoulders on the inner sides of the spinning sidebands suggest that there are two distinct bands of unequal intensity. These can be assigned to F coordinated by MgMgMg and MgMgSc respectively. Additional broadening in both spectra could be caused by dipolar coupling between nonbonded adjacent F atoms.

DISCUSSION

Synthesis

End-member pargasite was readily synthesized but yields were never quite 100%; minor phases could always be observed either in SEM photographs or in powder-diffraction patterns. However, all pargasite studies give fairly consistent results, and the cell dimensions reported by most studies are fairly close. Ignoring the outlying values, the total spread on each of the axial lengths is ≤0.3%; the precision reported would suggest that some of this scatter may be real. Incomplete yields always allow the possibility that the amphibole may deviate from nominal composition, and this was shown to be the case for pargasites in which Cr, Ga, and Sc substitute for ^{VI}Al. However, there is no direct confirmation of this in pargasite itself; the presence of minor additional phases does suggest that some of the pargasites may be off-composition. However, Charles (1980) reported yields of (nominal) pargasite from 60–99%, with pyroxene and plagioclase always present; despite this variation, the cell dimensions do not vary significantly with yield, suggesting (Charles, 1980) that either pargasites from charges with low amphibole yields are "off-composition" with cell dimensions fortuitously close to those from higher yield runs, or that the amphibole is "on-composition" despite the modal variations in the run products. Even when am-

phibole yields were about 99%, there was always some material observable by SEM that appeared not to be amphibole. It is possible that this small amount of other phase(s) was due to starting-mix contamination during the preparation procedure or to the minor contaminants always present in reagent-grade materials.

Substitution of Cr^{3+}, Ga, Sc, and In for ^{VI}Al reduced yields to 80–90%, and additional phases were prominent in the powder-diffraction patterns. Deviation from nominal composition was demonstrated by the infrared spectra of this series, all of which showed MgMgAl bands in addition to the $MgMgM^{3+}$ bands in the principal hydroxyl-stretching region (Figs. 3, 4). In addition, the total Sc content of the scandium-pargasite was derived from the Rietveld structure refinement (0.65 atoms pfu); the nominal value is 1.0, indicating an ^{VI}Al content of 0.35 atoms pfu. Another indication of compositional deviation from nominality is given by the type I stability diagram for this series. Prewitt and Shannon (1969) have shown that in an isostructural series, the cell volume is a linear function of the cube of the octahedral radius of the variable cation. Although Hawthorne (1978) has shown that this relationship is intrinsically nonlinear, the variation in cation radius in this series is sufficiently small that the linear model is adequate. Because the occupancy of the variable cation was generally less than nominal, this plot was modified to include the cubed average of all octahedral cation radii calculated from site occupancies. Figure 11 shows this diagram for the pargasites synthesized here; the ideal line is drawn through pargasite and through the datum point for the scandium-pargasite using its Rietveld-derived composition. As is apparent from Figure 11, pargasites with Cr and Ga substituted for ^{VI}Al lie off the line, showing that they deviate from their nominal composition. This argument does assume that the A site remains full (and hence the volume changes are not a function of A site occupancy). In the pargasites with Cr and Ga, there are no A-site vacant bands of any significance in the infrared spectra, indicating that the A sites are almost or completely filled; the pargasite itself may be an exception with its weak shoulder at about 3645 cm^{-1}. In addition, the deficiency of substituent cations in the octahedral strip could not be compensated by variable alkalis at the A site, as the charge variation is in the wrong sense. Consequently, these pargasites should contain significant ^{VI}Al that is not indicated by their nominal compositions.

The results of fluor-pargasite syntheses largely paralleled those of hydroxy-pargasites, except for higher yields of the scandium-fluor-pargasite compared to scandium-pargasite. The complete series of Ga, Cr, and Sc substitutions for octahedral Al was characterized by Rietveld structure refinement. Site occupancies (Table 7) show that chromium-fluor-pargasite and gallium-fluor-pargasite are deficient in Cr and Ga, respectively, compared to the nominal composition, but that scandium-fluor-pargasite has nearly the ideal Sc content. Variation of cell volume with the cube of the average octahedral cation radius (Fig. 11) is not linear, but is improved over hydroxy-pargasites.

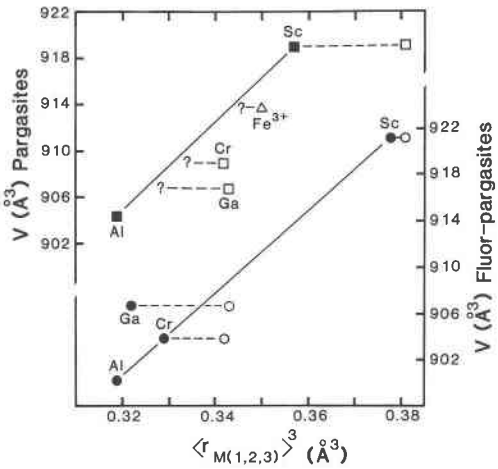

Fig. 11. Cell volume vs. the cube of average octahedral cation radius for pargasites (squares) and fluor-pargasites (circles). The hollow triangle represents magnesio-hastingsite synthesized on the cuprite-tenorite buffer (Semet, 1973). The hollow symbols denote nominal compositions, the filled symbols denote compositions derived from the Rietveld site-occupancy refinements; pargasite and fluor-pargasite are presumed to be "on composition."

Cation ordering

Much effort was expended on these pargasite series not only because of the success of previous work, but also because this composition is intrinsically interesting with respect to M^{3+} ordering at the octahedral sites and Al ordering at the tetrahedral sites.

For the pargasites, the infrared spectra (Fig. 3) show that the octahedrally coordinated trivalent cations were significantly disordered over the M(1,2,3) sites of the octahedral strip. There was a significant change in the ratio of the $MgMgM^{3+}$: MgMgMg band intensities across the series. This could be caused by changes in both ordering and clustering of cations coordinated to the hydroxyl and, in the absence of a specific model for clustering, cannot be used to derive the degree of ordering (Whittaker, 1979). It is extremely interesting that in natural pargasites, the octahedrally coordinated trivalent cations are nearly completely or completely ordered at M(2), whereas these synthetic pargasites were significantly disordered. We tried to determine if this was a kinetic effect by comparing synthesis runs of 27 and 1126 h. There was no discernible difference in the infrared spectra of these two run products; the product of the longer run might have been slightly coarser in grain size, but even this was difficult to decide. In addition, infrared spectra of pargasites (PA-A2A, PA-A8A, Table 1) annealed for 891 h at 500 and 590°C, respectively, were identical to spectra collected before annealing. Consequently, if the ordering of M^{3+} at M(2) in natural amphiboles is a postcrystallization effect, the kinetics were far too slow for it to be observed in our ex-

periments. Conversely, if the natural pargasites crystallized in an ordered configuration, the reasons for the difference in the ordering patterns of the natural and synthetic amphiboles are certainly not clear at present.

In the fluor-pargasites, the trivalent cations (with the exception of Al for which we have no information) tended to be more strongly ordered at M(2) than in the pargasites. Rosenberg and Foit (1977) observed similar behavior for Fe^{2+} in amphiboles and micas, whereby Fe^{2+} and, apparently, Cr^{3+}, Ga, and Sc avoid sites coordinated by F anions.

The results for the possible order-disorder relationships for tetrahedrally coordinated Al are much more ambiguous. In general, the ⟨T–O⟩ distances (Table 5) from the Rietveld refinements indicate complete ordering of ^{IV}Al at T(1) (except for gallium-fluor-pargasite). However, the individual T–O distances are known to be strongly affected during the refinement by local pseudosymmetry, and seem to be very imprecise. Thus the significance of the ⟨T–O⟩ values is questionable.

The ^{29}Si spectrum seems incompatible with complete ordering of ^{IV}Al at T(1), as this should give two or three well-separated peaks. The component peak intensities are sensitive to both ordering and clustering, and calculation of site occupancies from component peak intensities may require additional techniques sensitive to Al-Si ordering.

Conclusions

The present study has underlined the importance of detailed characterization of amphibole synthesis products, particularly with regard to cation order-disorder relationships. Of particular interest are the following points:

1. Infrared spectroscopy in the hydroxyl-stretching region is a rapid and versatile technique in the characterization of cation order-disorder at the M(1) and M(3) sites in synthetic amphiboles. Furthermore, deviations from nominal composition can also be revealed with some sensitivity.

2. Rietveld structure refinement can be used to characterize cation order-disorder when there is a significant difference in the scattering power of the constituent cations. This is particularly useful for fluor-amphibole work in which infrared spectroscopy cannot be used for this purpose.

3. The MAS NMR ^{29}Si spectrum shows good agreement with models involving Al disorder over the T(1) and T(2) sites, with best agreement for a model involving no ^{IV}Al–O–^{IV}Al linkages. However, these results cannot be regarded as conclusive because of the complex spectrum overlap and the unknown effect of octahedral-cation variation on the spectrum.

4. The characterization methods used in this work have shown that the amphiboles synthesized have ordering patterns distinctly different from their natural analogues. The proper characterization of these products assumes additional importance if thermodynamic properties are to be measured, as the present work shows that the state of order in a synthetic amphibole cannot be assumed by analogy with natural minerals.

Acknowledgments

Financial assistance was provided by the Natural Sciences and Engineering Research Council of Canada in the form of operating grants to A. C. Turnock, F. C. Hawthorne, and J. S. Hartman. B. L. Sherriff was supported by an Ontario Graduate Fellowship. We thank C. A. Fyfe, G. J. Kennedy, and R. E. Lenkinski of the University of Guelph for assistance with instrumentation and the Southwestern Ontario High Field NMR Centre for instrument time. We thank David M. Jenkins and an anonymous reviewer for thorough reviews of the original manuscript.

References

Appleman, D.E., and Evans, H.T. (1973) Job 9214: Indexing and least-squares refinement of powder diffraction data. U.S. National Technical Information Service, Document PB 216 188.

Boyd, F.R. (1954) Amphiboles. Carnegie Institution of Washington Year Book 53, 108–111.

——— (1959) Hydrothermal investigations of amphiboles. In P.H. Abelson, Ed., Researches in geochemistry, p. 377–396. Wiley, New York.

Braue, Wolfgang, and Seck, H.A. (1977) Stability of pargasite-richterite solid solutions at 1 kb water vapor pressure. Neues Jahrbuch für Mineralogie, Abhandlungen, 130, 19–32.

Charles, R.W. (1980) Amphiboles on the join pargasite-ferropargasite. American Mineralogist, 65, 996–1001.

Finger, L.W. (1969) Determination of cation distribution by least-squares refinement of single-crystal X-ray data. Carnegie Institution of Washington Year Book 67, 216–217.

Fyfe, C.A., Gobbi, G.C., Hartman, J.S., Lenkinski, R.E., O'Brien, J.S., Beange, E.R., and Smith, M.A.R. (1982) High resolution solid state MAS spectra of ^{29}Si, ^{27}Al, ^{11}B and other nuclei in inorganic systems using a narrow bore 400 MHz high resolution NMR spectrometer. Journal of Magnetic Resonance, 47, 168–178.

Gilbert, M.C. (1969) Reconnaissance study of the stability of amphiboles at high pressure. Carnegie Institution of Washington Year Book 67, 167–170.

Hamilton, D.L., and Henderson, C.M.B. (1968) The preparation of silicate compositions by a gelling method. Mineralogical Magazine, 36, 832–838.

Hawthorne, F.C. (1978) The relationship between cell volume, mean bondlength and effective ionic radius. Acta Crystallographica, A34, 139–140.

——— (1983a) Quantitative characterization of site-occupancies in minerals. American Mineralogist, 68, 287–306.

——— (1983b) The crystal chemistry of the amphiboles. Canadian Mineralogist, 21, 173–480.

Hawthorne, F.C., Raudsepp, Mati, Williams, B.L., and Hartman, J.S. (1984) Characterization of cation ordering in synthetic amphiboles by Rietveld structure refinement and ^{27}Al and ^{29} Si MAS NMR spectroscopy. Geological Association of Canada/Mineralogical Association of Canada Program with Abstracts, 9, 72.

Hinrichsen, Thomas, and Schürmann, Kay (1977) Experimental investigations on the Na/K substitution in edenites and pargasites. Neues Jahrbuch für Mineralogie, Abhandlungen, 130, 12–18.

Holloway, J.R. (1973) The system pargasite-H_2O-CO_2: A model for melting of a hydrous mineral with a mixed-volatile fluid—I. Experimental results to 8 kbar. Geochimica et Cosmochimica Acta, 37, 651–666.

Janes, Nathan, and Oldfield, Eric. (1985) Prediction of silicon-29 nuclear magnetic resonance chemical shifts using a group electronegativity approach. Applications to silicate and aluminosilicate structures. American Chemical Society Journal, 107, 6769–6775.

Lippmaa, E., Mägi, M., Samoson, A., Engelhardt, G., and Grimmer, A.-R. (1980) Structural studies of silicates by solid state high-resolution ^{29}Si NMR. American Chemical Society Journal, 102, 4889–4893.

Mägi, M., Lippmaa, E., Samoson, A., Engelhardt, G., and Grimmer, A.-R. (1984) Solid-state high-resolution silicon-29 chemical shifts in silicates. Journal of Physical Chemistry, 88, 1518–1522.

Maresch, W.V., and Czank, Michael. (1983) Phase characterization of

synthetic amphiboles on the join $Mn_2^{2+}Mg_{7-x}[Si_8O_{22}](OH)_2$. American Mineralogist, 68, 744–753.

Mueller, D., Gessner, W., Behrens, H.J., and Scheller, G. (1981) Determination of the aluminum coordination in aluminum-oxygen compounds by solid state high resolution ^{27}Al NMR. Chemical Physics Letters, 79, 59–62.

Oba, Takanobu. (1980) Phase relations on the tremolite-pargasite join. Contributions to Mineralogy and Petrology, 71, 247–256.

Prewitt, C.T., and Shannon, R.D. (1969) Use of radii as an aid to understanding the crystal chemistry of high pressure phases. American Crystallographic Association Transactions, 5, 51–60.

Raudsepp, Mati. (1984) Evaluation of amphibole synthesis and product characterization. Ph.D. thesis, University of Manitoba, Winnipeg.

Raudsepp, Mati, Turnock, A.C., and Hawthorne, F.C. (1982) Synthesis and characterization of $^{vi}R^{3+}$ analogues of pargasite and eckermannite. Geological Association of Canada/Mineralogical Association of Canada Program with Abstracts, 7, 75.

Raudsepp, Mati, Hawthorne, F.C., and Turnock, A.C. (1984) Derivation of site-occupancies in synthetic pyroxenes and amphiboles by Rietveld structure refinement. Geological Society of America Abstracts with Programs, 16, 630.

Rietveld, H.M. (1967) Line profiles of neutron powder-diffraction peaks for structure refinement. Acta Crystallographica, 22, 151–152.

——— (1969) A profile refinement method for nuclear and magnetic structures. Journal of Applied Crystallography, 2, 65–71.

Rosenberg, P.E., and Foit, F.F. (1977) Fe^{2+}-F avoidance in silicates. Geochimica et Cosmochimica Acta, 41, 345–346.

Schairer, J.F., and Bowen, N.L. (1955) The system K_2O-Al_2O_3-SiO_2. American Journal of Science, 245, 193–204.

Semet, M.P. (1973) A crystal-chemical study of synthetic magnesiohastingsite. American Mineralogist, 58, 480–494.

Smith, K.A., Kirkpatrick, R.J., Oldfield, Eric, and Henderson, D.M. (1983) High-resolution silicon-29 nuclear magnetic resonance spectroscopic study of rock-forming silicates. American Mineralogist, 68, 1206–1215.

Strens, R.G.J. (1974) The common chain, ribbon, and ring silicates. In V.C. Farmer, Ed., Infrared spectra of minerals. Mineralogical Society, London.

Veblen, D.R. (1981) Non-classical pyriboles and polysomatic reactions in biopyriboles. Mineralogical Society of America Reviews in Mineralogy, 9A, 189–236.

Westrich, H.R., and Holloway, J.R. (1981) Experimental dehydration of pargasite and calculation of its entropy and Gibbs energy. American Journal of Science, 281, 922–934.

Westrich, H.R., and Navrotsky, Alexandra. (1981) Some thermodynamic properties of fluorapatite, fluorpargasite, and fluorphlogopite. American Journal of Science, 281, 1091–1103.

Whittaker, E.J.W. (1979) Clustering of cations in amphiboles. Physics and Chemistry of Minerals, 4, 1–10.

Wiles, D.B., and Young, R.A. (1981) A new computer program for Rietveld analysis of X-ray powder diffraction patterns. Journal of Applied Crystallography, 14, 149–151.

Young, R.A. (1980) Structural analysis from X-ray powder diffraction patterns with the Rietveld method. Symposium on Accuracy in Powder Diffraction, National Bureau of Standards, Gaithersburg, Maryland, 143–163.

Young, R.A., and Wiles, D.B. (1981) Application of the Rietveld method for structure refinement with powder diffraction data. Advances in X-ray Analysis, 24, 1–23.

Manuscript received May 29, 1986
Manuscript accepted January 17, 1987